Role of crystalline precipitates on the mechanical properties of $(Cu_{0.50}Zr_{0.50})_{100-x}Al_x$ (x = 4, 5, 7) bulk metallic glasses

A. Castellero [a,*], T.A. Baser [a,b], J. Das [c,d], P. Matteis [e], J. Eckert [c,f], L. Battezzati [a], M. Baricco [a]

[a] Dipartimento di Chimica IFM and NIS, Università di Torino, Via P. Giuria 9, I-10125 Torino, Italy
[b] EMPA – Swiss Federal Laboratories for Materials Testing and Research, Dübendorf, Switzerland
[c] IFW Dresden, Institut für Komplexe Materialien, Helmholtzstr. 20, D-01069 Dresden, Germany
[d] Department of Metallurgical and Materials Engineering, Indian Institute of Technology, Kharagpur 721 302, West Bengal, India
[e] DISMIC – Politecnico di Torino, Corso Duca degli Abruzzi 24, I-10129 Torino, Italy
[f] TU Dresden, Institut für Werkstoffwissenschaft, D-01062 Dresden, Germany

ARTICLE INFO

ABSTRACT

The mechanical behaviour upon compression of $(Cu_{0.50}Zr_{0.50})_{100-x}Al_x$ (x = 4, 5, 7) rods with 2 and 3 mm diameter was systematically studied and compared with the literature data. Fully amorphous bulk metallic glasses (x = 5, 7) show little permanent deformation and reproducible yield stress values. The remarkable fracture strain, observed for some apparently X-ray diffraction amorphous samples (x = 4), was found to be due to significant amounts (at least 20%) of the B2-CuZr crystalline phase. The effect of possible flaws on the external surface of the rods was evaluated by mechanical testing of either as cast and machined samples.

© 2011 Elsevier B.V. All rights reserved.

1. Introduction

Bulk metallic glasses (BMGs), or amorphous alloys, exhibit unique mechanical properties, such as high yield strength and large elastic strain limit, together with relatively low Young's modulus [1]. However, BMGs do not show plasticity in tension due to shear softening (i.e. plastic deformation occurring along bands with lowered viscosity [2]). It is still an open debate if the permanent deformation which can be observed in bending and under compression can be truly called "ductility" [3,4], since the deformation occurs through a stick and slip process that produces a sequence of elastic deformations followed by local fractures which is manifested as a serrated flow in the stress–strain curves [5] until final failure occurs.

Improvement of the plasticity in BMGs can be achieved, typically upon compression, by introducing second phase particles such as ex situ ceramic particles [6], in situ coarse dendrites [7] or nanocrystalline precipitates [8–10], provided that a strong and intimate interface with the amorphous matrix is formed. The main role of the second phase particles is to favour the shear delocalisation by branching individual shear bands and stopping their propagation.

The presence of a stress concentration at the interface between the second phase particles and the amorphous matrix promotes the multiple shear initiation [11].

The strain at failure of BMG composites is strongly affected by the volume fraction of the second phase crystalline particles, the size of the particles and their dispersion in the amorphous matrix. On the one hand, in composites containing highly dispersed micron size ductile crystalline particles (e.g. dendrites) the shear band propagation is confined by the particle spacing, λ [7]. Furthermore, the ductile crystalline particles locally deform by dislocation mechanism [12], allowing plastic deformation either in compression and tension [11]. On the other hand, a finer dispersion of nanocrystalline particles tends to favour the initiation of multiple shear bands, but is little effective on stopping their propagation because the particles size is of the same order of magnitude with respect to the shear band width [9,11].

The unusual large "ductility" and work-hardening behaviour observed in $Cu_{47.5}Zr_{47.5}Al_5$ BMG [13], that was ascribed to the presence of nanoscale chemical heterogeneities, produced a wide interest in the mechanical properties of the Cu–Zr–Al BMGs. Rather scattered values of the yield stress, $\sigma_{0.2}$, (from 1550 MPa to 2050 MPa) and the fracture strain, ε_f, (from 2.5% to 18%) were found for $Cu_{47.5}Zr_{47.5}Al_5$ in the literature [13–18]. A slightly lower dispersion of the values of $\sigma_{0.2}$ (1600–1900 MPa) and ε_f (2–14.5%) was found in the case of $Cu_{46.5}Zr_{46.5}Al_7$ [19,20], $Cu_{46}Zr_{47}Al_7$ [21–28]

* Corresponding author. Tel.: +39 011 670 7097; fax: +39 011 670 7855.
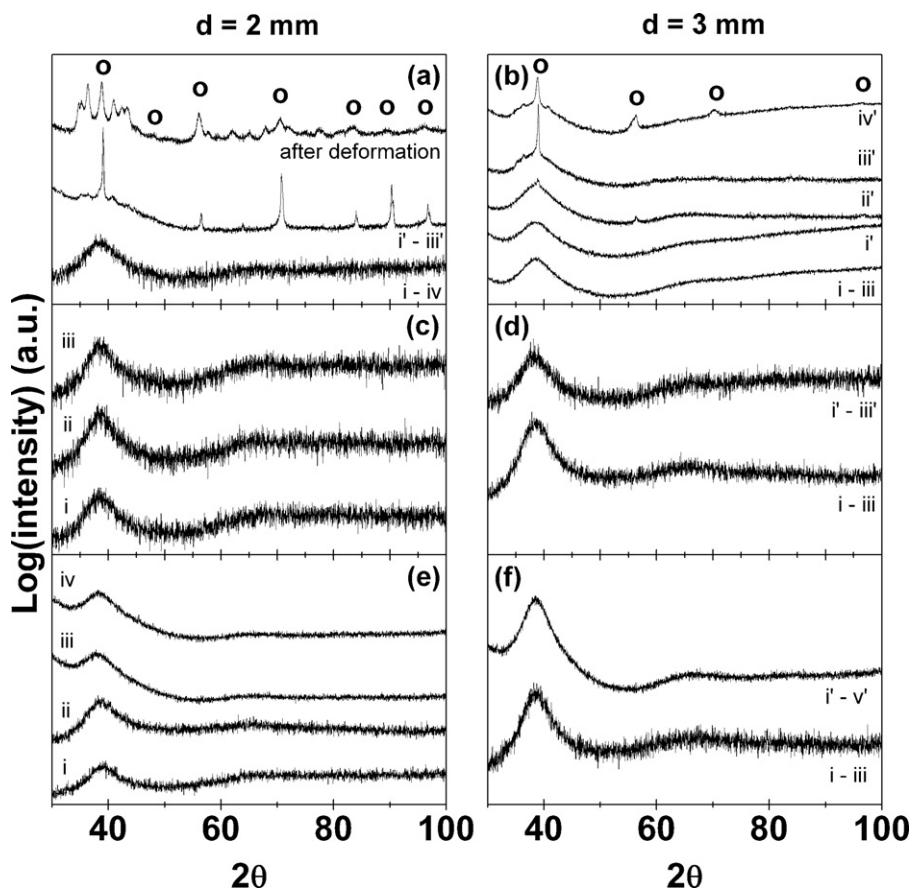E-mail address: alberto.castellero@unito.it (A. Castellero).

Fig. 1. Selected XRD patterns of different sections cut from the as cast rods. (a) and (b): $Cu_{48}Zr_{48}Al_4$ with 2 and 3 mm diameter, respectively; (c) and (d): $Cu_{47.5}Zr_{47.5}Al_5$ with 2 and 3 mm diameter, respectively; (e) and (f): $Cu_{46.5}Zr_{46.5}Al_7$ with 2 and 3 mm diameter, respectively.

and $Cu_{47}Zr_{47}Al_6$ [29,30], which will be considered as a single composition in this work.

The variability of the BMGs behaviour under compression, typical of intrinsically brittle materials, recently stimulated the study of statistical [4,31] and geometric effects [4,32] in order to achieve a more comprehensive and critical understanding of the mechanical properties of amorphous alloys.

According to Ref. [4], a statistical analysis of the fracture stress dispersion based on the Weibull approach showed that BMGs have a Weibull modulus higher than brittle ceramics resulting, therefore, mechanically more reliable. Furthermore, different values of the Weibull modulus allow also to distinguish between brittle and "ductile" BMGs. It was also shown [4,32] that unusual large compressive strain can be due to geometrical constrains related to the aspect ratio (<2) or to the presence of imperfections in the sample geometry (e.g. non-orthogonal specimens).

In this paper, the mechanical properties of $(Cu_{0.50}Zr_{0.50})_{100-x}Al_x$ ($x = 4, 5, 7$) BMGs were studied under compressive load by testing different sections along the length of the as cast rods. Microstructures and fracture surfaces of the compressed samples were observed by optical microscopy and scanning electron microscopy, respectively. The correlation between microstructure, external surface quality and compressive plasticity is discussed.

2. Experimental

Master alloy ingots with $Cu_{48}Zr_{48}Al_4$, $Cu_{47.5}Zr_{47.5}Al_5$ and $Cu_{46.5}Zr_{46.5}Al_7$ nominal composition (at.%) were prepared by arc melting the pure elements under Ar atmosphere. Each ingot was remelted several times in order to obtain a good homogeneity. 2 and 3 mm diameter rods were produced by injection casting into copper moulds with a Bühler D-7454 machine using a quartz crucible. Several sections were obtained from each as cast rod and progressively labelled from the bottom

as follows: $Al_x\text{-}y\_z$, where ($x = 4, 5$ and 7), ($y = 2$ and 3) and ($z = $ i, ii, iii, etc.) indicate the atomic percent of Al in the alloy, the rod diameter and the position in the rod, respectively. The surface roughness of the as cast rods was evaluated by means of a TESA-Rugosurf 90G roughness tester according to the ISO 4287 standard. A Panalytical X'Pert X-ray diffractometer (XRD) with Cu Kα radiation was used for structural characterisation. In order to evaluate the mechanical properties under compression, cylindrical specimens with 2:1 aspect ratio were tested with an Instron 8562 testing machine at initial strain rate of 2×10^{-4} s^{-1}. The bottom and the top surfaces of the each section were carefully polished in order to make them parallel and perpendicular to the loading axis before the compression test. In the case of $Cu_{46.5}Zr_{46.5}Al_7$ 3 mm rod, the effect of the external surface quality on the mechanical properties was evaluated by testing either samples in the as cast conditions and specimens whose surface was machined in order to remove possible flaws (with consequent reduction of the sample diameter down to 2.7 mm). Fractured surfaces have been observed by Leica Stereoscan 410 scanning electron microscope (SEM). Crystalline fractions were determined by metallographic observations using a Leica optical microscope after mirror polishing and chemical etching with an aqueous solution of 20% HF and 1% HNO$_3$.

The crystals distribution in the amorphous matrix was evaluated by calculating the mean free distance, λ, between the crystals according to Ref. [33]:

$$\lambda = \frac{1 - (V_V)_{cryst}}{(N_L)_{cryst}} \tag{1}$$

where $(V_V)_{cryst}$ is the volume crystalline fraction and $(N_L)_{cryst}$ is the number of crystals intercepted per unit length of the test line:

$$(N_L)_{cryst} = \frac{2(P_L)_{cryst-cryst} + (P_L)_{cryst-am}}{2} \tag{2}$$

Eq. (2) refers to the more general case when the crystals are not always separated and the different types of interfaces that are intersected (crystal–crystal and crystal–amorphous) must be considered.

3. Results

Fig. 1 shows selected XRD patterns of the different sections cut from the as cast rods. In the case of $Cu_{48}Zr_{48}Al_4$, the sections

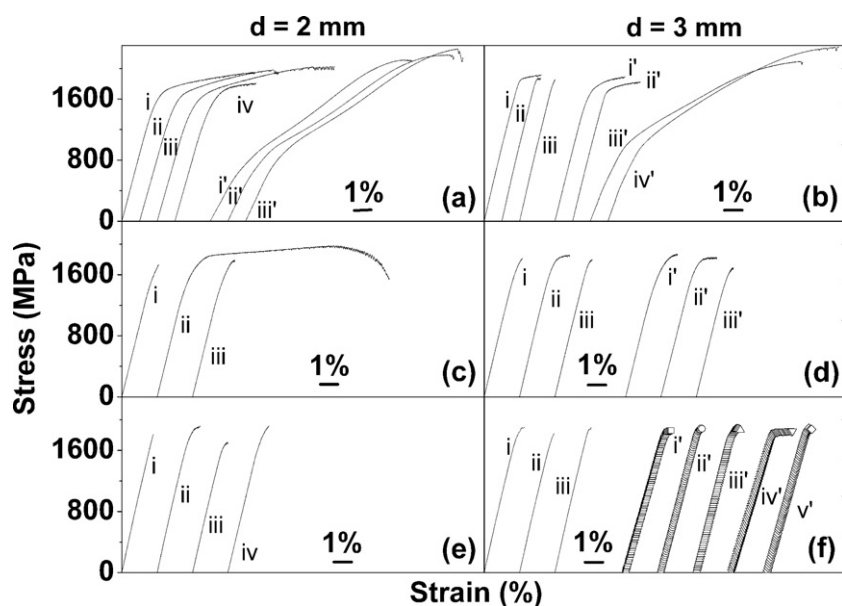**Fig. 2.** Stress–strain compression curves of the all rods tested. (a) and (b) $Cu_{48}Zr_{48}Al_4$ with 2 and 3 mm diameter, respectively; (c) and (d) $Cu_{47.5}Zr_{47.5}Al_5$ with 2 and 3 mm diameter, respectively; (e) and (f) $Cu_{46.5}Zr_{46.5}Al_7$ with 2 and 3 mm diameter, respectively. Continuous lines and symbols indicate as cast and machined samples, respectively.

obtained from different rods either with diameter 2 and 3 mm gave different results: Al_4-2_(i–iv), Fig. 1(a), and Al_4-3_(i–iii), Fig. 1(b) shows an amorphous halo without any evidence of diffraction peaks, suggesting a fully amorphous structure. However, the XRD pattern representative of Al_4-2_(i'–iii'), Fig. 1(a) shows crystallographic reflections belonging to the B2-CsCl type phase CuZr [34], marked with the open circles, and to a monoclinic martensitic phase (remaining unmarked peaks) [35]. In the case of Al_4-3_(i'–iv'), a progressive increase of the crystalline fraction from the bottom (X-ray amorphous) to the top of the rod is observed, Fig. 1(b).

For $Cu_{47.5}Zr_{47.5}Al_5$, Fig. 1(c) and (d), and $Cu_{46.5}Zr_{46.5}Al_7$, Fig. 1(e) and (f), the XRD patterns show the typical amorphous halo for all the sections.

Fig. 2 shows the stress–strain curves, shifted for sake of clarity, obtained under compression for different specimens. Al_4-2_(i–iv) samples, which resulted to be X-ray amorphous, show a significant permanent deformation (between 5.5% and 8%) for the different sections of the rod. No significant variations in yield strength can be observed. The first, second and third sections show a significant "work hardening-like" behaviour, quite unusual for a metallic glass, up to 1953 MPa, 1984 MPa and 2021 MPa, respectively. In the case of Al_4-2_(i'–iii'), containing the crystalline phase B2-CuZr, the yield stress is significantly lowered and the plastic deformation raises up to 10% after a remarkable work-hardening. For the 3 mm diameter samples, Al_4-3_(i'–iv') show a progressively reduction of the yield stress and increase of the deformation as the crystalline fraction increases. Finally, Al_4-3_(i–iii) show a poorer deformation and a higher yield stress with respect the all the other sections with the same composition previously described.

XRD analysis of the sample Al_4-2_(i'–iii') after deformation, Fig. 1(a) shows that the peaks belonging to the martensitic phase grow suggesting a deformation induced martensitic transformation of B2-CuZr in accordance with previous findings [36].

In the case of $Cu_{47.5}Zr_{47.5}Al_5$ and $Cu_{46.5}Zr_{46.5}Al_7$, all the sections tested show a quite poor permanent deformation (0–1.5%) and rather comparable values of the yield stress. An exception is given by Al_5-2_ii, whose remarkable deformation was due to the non-perfect parallelism of the two bases and consequently to a non uniaxial loading. The data obtained for this sample were not considered in the following of this work.

In order to shed light upon the different mechanical behaviour of specimens that apparently seem to be structurally equivalent (i.e. fully amorphous), these were grinded, mirror polished and chemically etched in order to expose the longitudinal section, parallel to the loading axis, in correspondence of the half of the samples.

The findings of the metallographic observations are summarised in Fig. 3. The micrograph in Fig. 3(a), representative of the samples Al_4-2_(i'–iii') and Al_4-3_(iii'–iv'), clearly shows that these contain a preponderant fraction (79–96%) of a homogeneously distributed crystalline phase, as expected from the corresponding XRD patterns. In the case of the samples Al_4-2_(i–iv), which appear to be X-ray amorphous, the metallographic observations surprisingly show a significant fraction (19–23%) of large and inhomogeneously distributed crystals with dendritic morphology, belonging to the B2-CuZr phase, as shown in Fig. 3(b). The apparent fully amorphous structure detected by XRD for the Al_4-2_(i–iv) samples, Fig. 1(a), is due to the non uniform distribution of large crystals, which reduces the chance of detecting them by mean of this technique.

Fig. 3(c) and (d) shows that, for Al_4-3_(i'–ii') and Al_4-3_(i–iii) respectively, the crystalline fraction is significantly lower (3–8%). In both cases the B2-CuZr crystals are homogeneously distributed in the amorphous matrix, however a finer dispersion of smaller crystals ($\leq 10^\circ \mu$m) can be observed in Fig. 3(d). In the case of $Cu_{47.5}Zr_{47.5}Al_5$ and $Cu_{46.5}Zr_{46.5}Al_7$, all the sections show featureless microstructures, shown in Fig. 3(e), confirming that the samples are fully amorphous in accordance with the XRD results.

The values of the mean free distance, λ, calculated for Fig. 3(a)–(c), showing crystalline aggregates of the order of 10 μm and more, are 0.023 mm, 0.692 and 1.180 mm, respectively, and scale inversely with the crystalline fraction. In the case of Fig. 3(d), where the crystalline fraction is approximately the same (about 8%) as in Fig. 3(c) but there is a finer dispersion of smaller crystals (crystals size $\leq 10^\circ \mu$m), the value of λ decreases to 0.250 mm.

The SEM micrographs in Fig. 4(a)–(c), shows the fracture surfaces of samples with a progressive increase of the crystalline content, whose microstructure is shown in Fig. 3(e), Fig. 3(b) and Fig. 3(a), respectively. For the fully amorphous BMGs, Fig. 4(a), the fracture surface shows only the typical vein patterns. In the case of intermediate crystalline fraction (around 20%), Fig. 4(b), the surface fracture is mainly characterised by vein patterns and river patterns, related to the failure of the amorphous matrix, alternated to
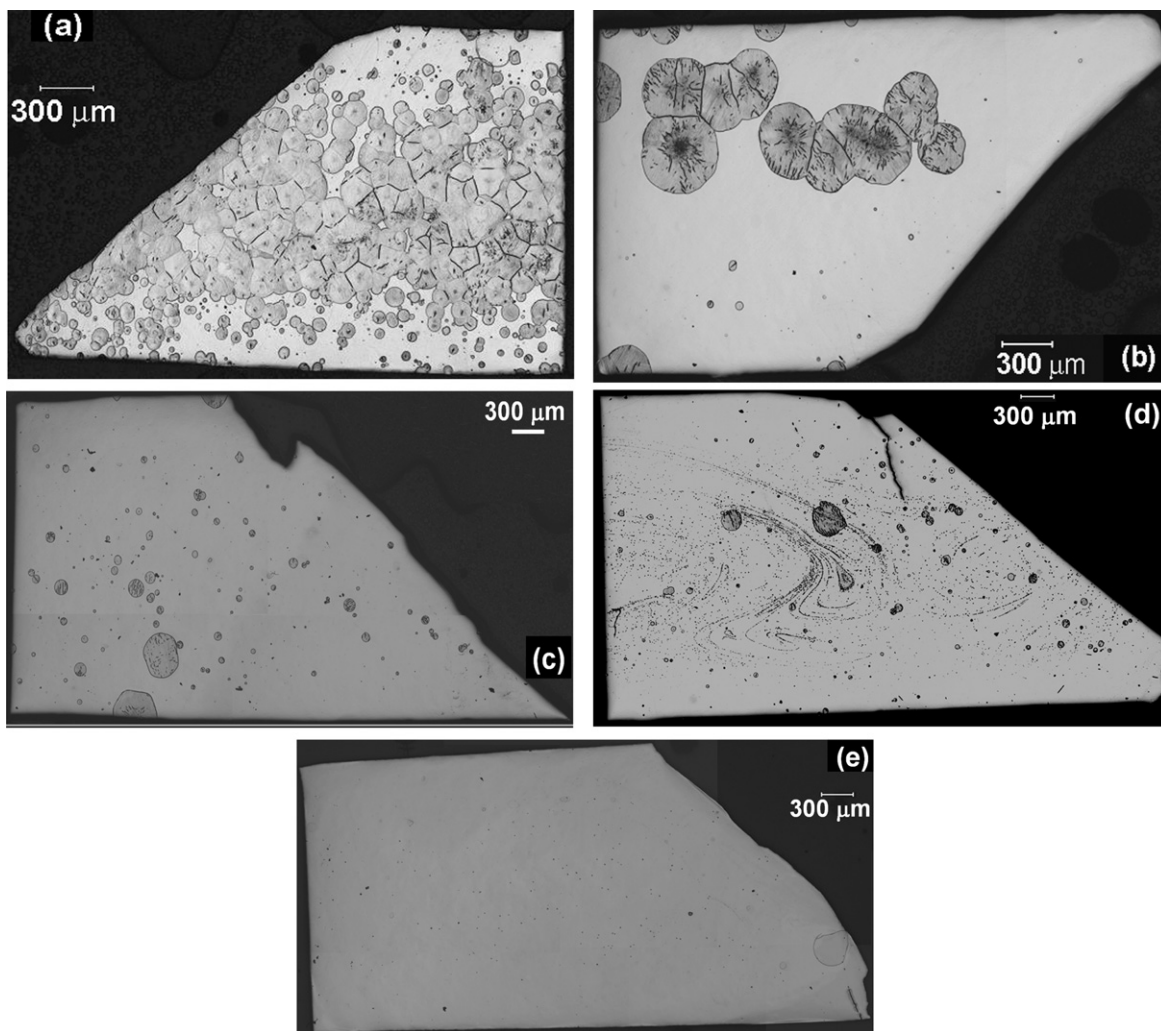
Fig. 3. Representative optical micrographs of the etched longitudinal sections (i.e. parallel to the loading axis) of the samples broken upon compression. (a): highly crystalline Al$_4$-2_(iii′). (b): partially crystalline (∼23%) Al$_4$-2_(i). (c): partially crystalline (∼8%) Al$_4$-3_(i). (d) partially crystalline (∼8%) Al$_4$-3_(i′). (e): fully amorphous Al$_5$-3_(i).

featureless regions. For high crystalline fraction (∼90%), Fig. 4(c), an irregular fracture surface characterised by the alternation of smooth and rough regions and the random presence of river patterns is observed. Fig. 4(d), illustrating the external surface of the same sample of Fig. 4(c), shows that the propagation of shear bands through the amorphous matrix are stopped by the large crystals of B2-CuZr, which mainly support the deformation.

The large spread of crystalline fraction values in different rods with the same composition (Cu$_{48}$Zr$_{48}$Al$_4$) was found to be correlated with the roughness of the external surface of the as cast rods, which can be likely related to the finishing of the copper mould surface. For example, samples with 93%, 15% and 0% crystalline fractions show R_a values of 2.36 ± 0.49 μm, 0.34 ± 0.16 μm and 0.24 ± 0.09 μm, respectively. Such a trend is expected since a higher roughness promotes the heterogeneous nucleation on the mould surface, especially in the case of systems with a lower glass forming ability such as Cu$_{48}$Zr$_{48}$Al$_4$.

4. Discussion

The values of ε_f and $\sigma_{0.2}$ for Cu$_{47.5}$Zr$_{47.5}$Al$_5$ and Cu$_{46.5}$Zr$_{46.5}$Al$_7$ BMGs obtained in this work (open symbols) and taken from the literature (filled symbols) [13–30] are reported as a function of the sample diameter in Fig. 5(a) and (b), respectively. The values of the fracture strain measured in this work are less scattered with respect

to the values reported in the literature and do not show any clear trend with respect the sample size and the composition. Also our values of the yield stress for Cu$_{47.5}$Zr$_{47.5}$Al$_5$ and Cu$_{46.5}$Zr$_{46.5}$Al$_7$ are independent of the sample size, however Cu$_{47.5}$Zr$_{47.5}$Al$_5$ tend to yield at lower stress with respect to Cu$_{46.5}$Zr$_{46.5}$Al$_7$.

As already suggested in Ref. [37], some of the discrepancies in plasticity reported in the literature [13–18] for Cu$_{47.5}$Zr$_{47.5}$Al$_5$ BMG could be due to the presence of not irrelevant amounts of crystals that were not detected by laboratory scale XRD. Furthermore, it appears clear that plastic deformations higher than 3% and work hardening behaviour are observed only when considerable amounts of the B2-CuZr phase (at least 20%) are present.

The effect of the crystalline fraction, f_c, on ε_f and $\sigma_{0.2}$ for Cu$_{48}$Zr$_{48}$Al$_4$ is reported in Fig. 5(c) and (d), respectively. Since no fully amorphous sample could be obtained for Cu$_{48}$Zr$_{48}$Al$_4$, the values of ε_f and $\sigma_{0.2}$, used for $f_c = 0$ in Fig. 5(c) and (d) respectively, are the mean values obtained for Cu$_{47.5}$Zr$_{47.5}$Al$_5$ and Cu$_{46.5}$Zr$_{46.5}$Al$_7$. The fracture strain increases and the yield stress decreases continuously with the crystalline fraction. Since in the present set of data there are not experimental values of ε_f and $\sigma_{0.2}$ for intermediate crystalline fractions (30–60%), it is not possible to verify if there is a critical crystalline fraction (∼30%) which maximises the fracture strain due to the ideal interconnection between crystals and amorphous matrix, as shown in Ref. [37]. In Fig. 5(d) it is also reported the calculated values of $\sigma_{0.2}$ using the rule of mixture (ROM), solid
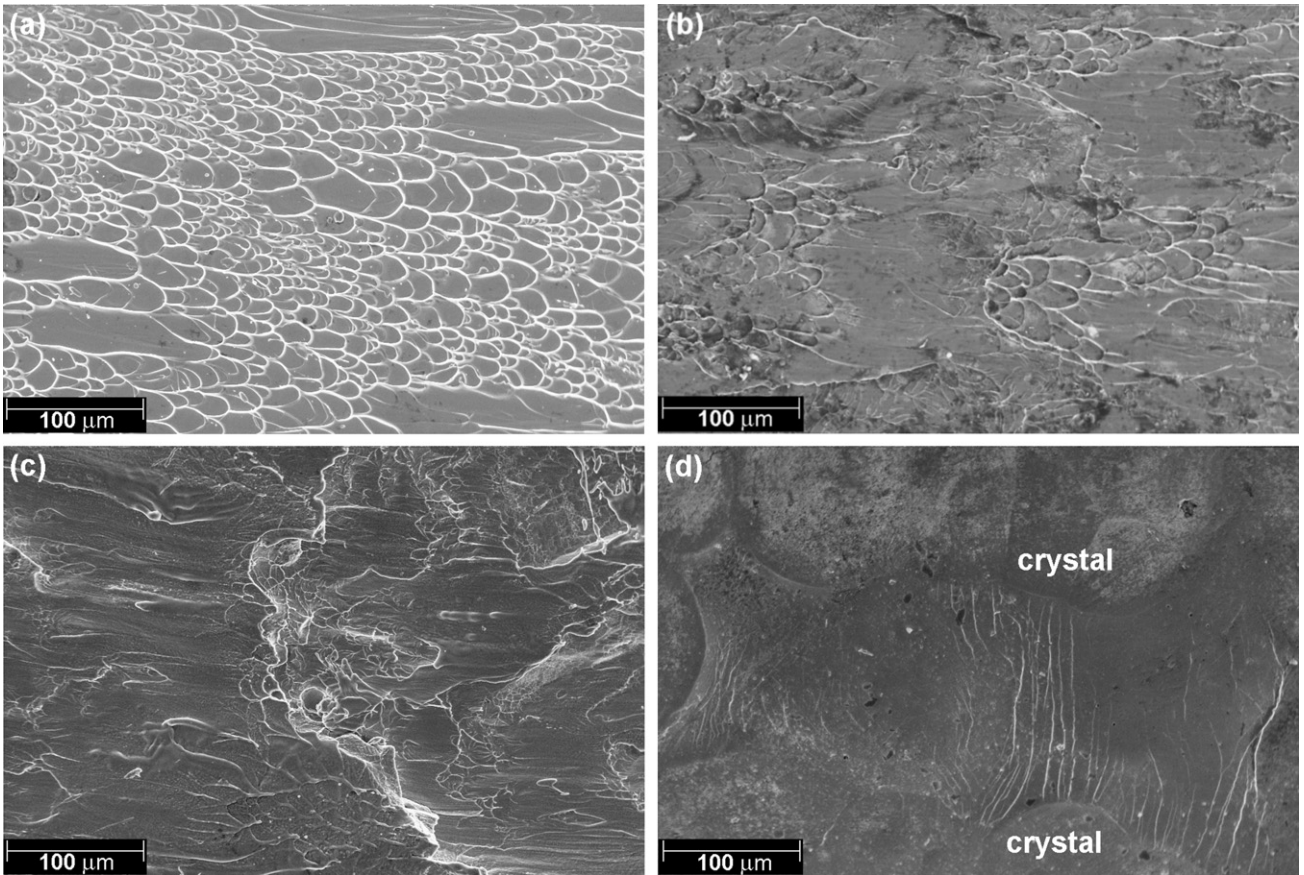
Fig. 4. Representative SEM fracture surfaces of the following samples: (a) fully amorphous Al_5-3_(i); (b), partially crystalline (∼23%) Al_4-2_(i); (c) highly crystalline Al_4-2_(iii′); (d) external surface of Al_4-2_(iii′), highly crystalline, undergone to compressive deformation.

line, and the load-bearing model, dotted line. It is evident that the values calculated with the ROM are in a good agreement with the experimental data. This is expected for composites in which the amount of one phase is significantly larger with respect the other,

like in our case, since the yield occurs is mainly controlled by the structure of the phase present in larger quantity:

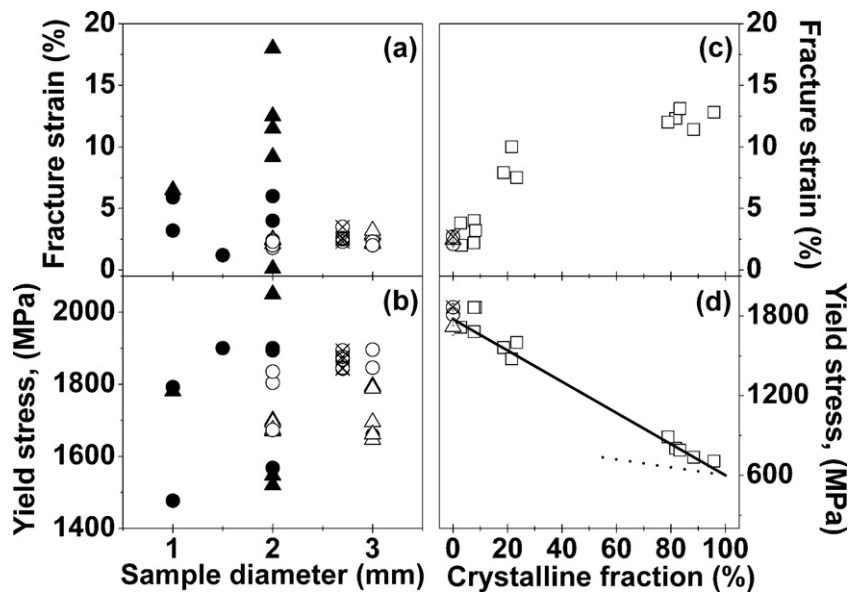$$\sigma_{composite} = f_{am}\sigma_{am} + f_{cryst}\sigma_{cryst} \tag{3}$$

Fig. 5. Fracture strain, (a) and yield stress, (b) of fully amorphous $Cu_{47.5}Zr_{47.5}Al_5$ and $Cu_{46.5}Zr_{46.5}Al_7$ as a function of sample diameter. Fracture strain, (c) and yield stress, (d) of $Cu_{48}Zr_{48}Al_4$ as a function of the crystalline fraction. Data marked by open symbols (squares, triangles, circles and crossed circles for as cast $Cu_{48}Zr_{48}Al_4$, as cast $Cu_{47.5}Zr_{47.5}Al_5$, as cast $Cu_{46.5}Zr_{46.5}Al_7$ and machined $Cu_{46.5}Zr_{46.5}Al_7$, respectively) are from this work. Filled symbols (triangle and circles for $Cu_{47.5}Zr_{47.5}Al_5$ and $Cu_{46.5}Zr_{46.5}Al_7$, respectively), indicate data from the literature [13–30].

where f and σ are the volume fraction and the yield stress, respectively, of the amorphous and crystalline phases. For the calculation values of 1800 MPa and 600 MPa were considered for the yield stress of the amorphous matrix and the crystalline phase, respectively.

Conversely, the values calculated with the load-bearing model [38] show a less satisfying agreement with the experimental data obtained for high crystalline fractions:

$$\sigma_{composite} = \sigma_{cryst}(1 + 0.5 f_{am}) \tag{4}$$

Because of the absence of experimental data for intermediate crystalline fractions (i.e. 30–60%), it is not possible to distinguish which of the two proposed models describes better the mechanical behaviour of the composite. According to Ref. [37], where a more complete set of data was available, it appears crucial the existence of a critical crystalline volume, in correspondence of the percolation threshold, that separates the regions where the deformation is dominated, on the one hand, by the amorphous matrix and, on the other hand, by the crystalline phase.

Furthermore, for low crystalline fraction (below 10%) the distribution of the second phase particles (estimated by means of the mean free distance between the particles, λ) in the amorphous matrix does not show any effect on the fracture strain. In fact, for such a low crystalline fraction the microstructure length scale (i.e. λ) is one order of magnitude larger than the length scale characteristic for the plastic deformation of metallic glasses [7].

Finally, in the case of the BMGs with 3 mm diameter, a comparison between the mechanical behaviour of the specimens in the as cast conditions ($Cu_{47.5}Zr_{47.5}Al_5$), $R_a = 0.24 \pm 0.09$ μm, and after surface machining ($Cu_{46.5}Zr_{46.5}Al_7$), $R_a = 0.19 \pm 0.01$ μm, was attempted by applying the Weibull analysis [39], even if the population was limited to 6 samples for each series and the compositions are different. The increase of the Weibull modulus from 34 (as cast) to 69 (after machining) suggests that a higher reliability of the BMGs mechanical properties can be attained by removing from the external surface possible flaws that can initiate a premature crack leading to failure.

5. Conclusions

The glass formation of $(Cu_{0.50}Zr_{0.50})_{100-x}Al_x$ ($x = 4, 5, 7$) alloys, prepared in rod form by injection casting, was investigated by X-ray diffraction and optical microscopy, while mechanical properties were studied by compression tests at room temperature. In the case of $Cu_{48}Zr_{48}Al_4$, relevant amount ($\sim 20\%$) of large and inhomogeneously distributed crystals, belonging to the B2-type CuZr phase, were detected by optical microscopy in X-ray amorphous samples. For this alloy, the large variation of the yield strength and fracture strain values can be explained by the presence of various amounts (from 3% to 96%) of micron-sized B2-CuZr crystals embedded in the amorphous matrix. Increasing the crystalline fraction, the permanent deformation increases and the yield stress decreases. In the case of the fully amorphous samples ($x = 5, 7$), the yield stress and fracture strain values were independent on the sample size and show little scatter.

Our findings suggest that the significant spread of fracture strain values reported in the literature for BMGs with the same compo-

sitions could be due to the microstructural inhomogeneity of the samples containing undetected amount of crystals, raising also a methodological issue for the proper structural characterisation of BMGs. In addition, a preliminary statistic analysis indicated that the reliability of BMGs mechanical properties can be improved by machining the as cast external surface with consequent removal of possible flaws.

References

[1] A. Inoue, Acta Mater. 48 (2000) 279.
[2] F. Spaepen, Acta Metall. 25 (1977) 407.
[3] J.J. Lewandowski, W.H. Wang, A.L. Greer, Phil. Mag. Lett. 85 (2005) 77.
[4] W.F. Wu, Y. Li, C.A. Schuh, Phil. Mag. 88 (2008) 71.
[5] W.J. Wright, R. Saha, W.D. Nix, Mater. Trans. 42 (2001) 642.
[6] F. Szuecs, C.P. Kim, W.L. Johnson, Acta Mater. 49 (2001) 1507.
[7] C.C. Hays, C.P. Kim, W.L. Johnson, Mater. Sci. Eng. A 304–306 (2001) 650.
[8] K.B. Kim, J. Das, F. Baier, M.B. Tang, W.H. Wang, J. Eckert, Appl. Phys. Lett. 88 (2006) 051911.
[9] A. Inoue, W. Zhang, T. Tsurui, A.R. Yavari, A.L. Greer, Phil. Mag. Lett. 85 (2005) 221.
[10] D.V. Louzguine-Luzgin, A. Vinogradov, A.R. Yavari, S. Li, G. Xie, A. Inoue, Phil. Mag. 88 (2008) 2979.
[11] C.A. Schuh, T.C. Hufnagel, U. Ramamurty, Acta Mater. 55 (2007) 4067.
[12] E. Pekarskaya, C.P. Kim, W.L. Johnson, J. Mater. Res. 9 (2001) 2513.
[13] J. Das, M.B. Tang, K.B. Kim, R. Theissmann, F. Baier, W.H. Wang, J. Eckert, Phys. Rev. Lett. 94 (2005) 205501.
[14] S.W. Lee, M.-Y. Huh, E. Fleury, J.-C. Lee, Acta Mater. 54 (2006) 349.
[15] G. Kumar, T. Ohkubo, T. Mukai, K. Hono, Scripta Mater. 57 (2007) 173.
[16] W. Jiang, H. Zhang, F. Liu, Y. Wang, H. Choo, P.K. Liaw, Adv. Eng. Mater. 9 (2007) 959.
[17] Q.P. Cao, J.F. Li, Y.H. Zhou, J.Z. Jiang, Scripta Mater. 59 (2008) 673.
[18] Z.W. Zhu, S.J. Zheng, H.F. Zhang, B.Z. Ding, Z.Q. Hu, P.K. Liaw, Y.D. Wang, Y. Ren, J. Mater. Res. 23 (2008) 941.
[19] T.L. Cheung, C.H. Shek, J. Alloys Compd. 434–435 (2007) 71.
[20] P. Matteis, P. Russo Spena, C. Pozzi, T.A. Baser, M. Baricco, L. Battezzati, D. Firrao, A. Castellero, Metall. Mater. Trans. A 41 (2010) 1767.
[21] D. Xu, G. Duan, W.L. Johnson, Phys. Rev. Lett. 92 (2004) 245504.
[22] E.S. Park, D.H. Kim, Acta Mater. 54 (2006) 2597.
[23] E.S. Park, J.S. Kyeong, D.H. Kim, Scripta Mater. 57 (2007) 49.
[24] J.T. Fan, Z.F. Zhang, F. Jiang, J. Sun, S.X. Mao, Mater. Sci. Eng. A 487 (2008) 144.
[25] L. Zhang, F. Jiang, D. Zhang, L. He, J. Sun, J. Fan, Z. Zhang, Adv. Eng. Mater. 10 (2008) 943.
[26] J. Pan, L. Liu, K.C. Chan, Scripta Mater. 60 (2009) 822.
[27] L.C. Zhang, F. Jiang, Y.L. Zhao, J.F. Zhang, L. He, J. Sun, Mater. Sci. Eng. A 527 (2010) 4122.
[28] J. Pan, K.C. Chan, Q. Chen, N. Li, S.F. Guo, L. Liu, J. Alloys Compd. 504 (2010) S74.
[29] C. Duhamel, J. Das, S. Pauly, K.S. Lee, J. Eckert, Rev. Adv. Mater. Sci. 18 (2008) 527.
[30] J. Das, S. Pauly, M. Boström, K. Durst, M. Göken, J. Eckert, J. Alloys Compd. 483 (2009) 97.
[31] Y.-Y. Zhao, E. Ma, J. Xu, Scripta Mater. 58 (2008) 496.
[32] K. Mondal, G. Kumar, T. Ohkubo, T. Oishi, K. Mukai, K. Hono, Phil. Mag. Lett. 87 (2007) 625.
[33] E.E. Underwood, Quantitative Stereology, Addison-Wesley Pub. Co., Reading (MA), U.S.A., 1970.
[34] E.M. Carvalho, I.R. Harris, J. Mater. Sci. 15 (1980) 1224.
[35] A. Zhalko-Titarenko, M. Yevlashina, V. Antonov, B. Yavorskii, Yu. Koval, G. Firstov, Phys. Status Solidi B 184 (1994) 121.
[36] S. Pauly, J. Das, J. Bednarcik, N. Mattern, K.B. Kim, D.H. Kim, J. Eckert, Scripta Mater. 60 (2009) 431.
[37] S. Pauly, G. Liu, G. Wang, U. Kühn, N. Mattern, J. Eckert, Acta Mater. 57 (2009) 5445.
[38] V.C. Tardone, K.M. Prewo, Scripta Metall. 20 (1986) 43.
[39] W. Weibull, J. Appl. Mech. 18 (1951) 293.